Phase Transitions in Porous Media

John Carpenter

May 2, 2000

Abstract

The effects of porous media on the phase transitions of various systems will be examined. Experimental work on fluids such as liquid crystals and superfluid helium will be reviewed from the standpoint of both first order and continuous transitions. Along with these, the structural properties of porous silicon will be discussed. Finally, we will inspect several theoretic and computational descriptions of the experimental systems from the view of mean field theory and Monte Carlo simulations.

1 Introduction

The use of porous media for many applications such as purification and filtration has persisted for many centuries and indeed much longer in nature itself. With the advances of the twentieth century in the description of phase transitions there has been a natural interest in the behavior of these transitions when a porous material is present. Indeed, upon discovery of the superfluid phase of helium, one of the first experiments, the superfluid fountain, involved the flow of the fluid through a porous powder [9]. Since this time, the discovery of new porous materials as well as new applications has led to a wide range of experimental and theoretical work. The useful applications range from the aforementioned filtration to catalysis, oil filtration, electronics, medicine, and many more. In the following pages the highlights of the recent work on phase transitions in porous media will be presented.

Before an understanding of the phenomena found in the transitions may be obtained, one must form a basic understanding of the materials involved. There are three main types of media found in experiments we will examine, Vycor, aerogel, and Anopore. Vycor is a porous glass produced in a two step process. First a borosilicate glass undergoes spinodal decomposition, and then the boron-rich phase is leached out [10]. This process results in a completely interconnected pore network with a narrow size distribution with a pore density, porosity, of about 30% [9].

Now aerogel is produced via the sol-gel process. This process involves first forming a silica gel and then extracting the solvent by hypercritically drying the sample. The result is a structure of silica strands connected at random sites. The porosity can range from 85 to 99.8 percent [11]. The strands of these aerogels have been found to exhibit fractal behavior over scales from one to several hundred nanometers [9].

The third type of porous media we will examine is Anopore. The porosity of Anopore falls roughly in between that of Vycor and aerogel, at approximately 54%. It is an electrochemically grown alumina filter material and has a pore size much

larger than either Vycor or aerogel. The main difference however, is that the pores are not cross-linked but instead are parallel to each other and perpendicular to the surface [10].

With these materials in mind, we will proceed to examine several examples of experimental phenomena (Section 2). These will fall into two basic categories. The first of these is transitions which involve a change in the porous material itself in which one has the example of porous silicon. The second category is that of transitions of the embedded material, in which the porous media remains fixed. First and second order transitions of various materials will be viewed in this context. In Section 3 then, several theoretical models of these transitions will be examined.

2 Experimental Work

One type of structural transition is the pressure induced transition of porous silicon. Now this material is not the same as aerogel, although it is also made of silicon. Porous silicon is prepared by anodic etching of n-type Si(100) wafers in hydrofluoric acid and ethanol [8]. This results in a porous material with a yellow-gold color. The interesting behavior of this material is that it luminesces with an energy that is greater than the indirect band gap of bulk silicon. Ryan, et. al. [8], found that as the pressure on the silicon was increased through approximately $170kbar$, its color changed to black for all higher pressures. Upon relief of the pressure, the silicon did not return to its original color, but rather an orange-red color and would no longer luminesce. It is believed that this transition is a parallel with a transition in bulk silicon to a metallic and then hexagonal structure at pressures of $120 - 150kbar$, implying that the porous silicon is actually composed of crystalline silicon.

The next set of phenomena we will examine are first order transitions. To begin, we consider the isotropic-nematic transition of liquid crystals. The isotropic phase has no orientational nor translational long-range order while the nematic phase has only orientational long-range order. This transition has been studied in aerogels

of varying porosity. The divergence of the heat capacity of the bulk liquid crystal is found to be shifted and reduced in magnitude for increasing aerogel density. Wu, et. al. [7] found that for densities of 0.08, 0.17, 0.36, and 0.60 the transition temperature was reduced by $0.45K$, $0.72K$, $1.31K$, and $2.58K$ respectively. By subtracting the background, the excess heat capacity heights may be compared. This data of Wu [7] is shown in Fig. 1. The attenuation for increasing density is quite clear. Of interest to note is that a second order nematic-smectic-A transition was also found to behave the same qualitatively [7].

One might reasonably suspect that these effects are due simply to the finite size of the pores in the aerogel. However, Wu, et. al. [7] found that the expected scaling laws were violated. Power laws were fit to the reduced temperature and excess heat capacity as functions of the average pore width and were found to be as follows, $t \propto L^{-1}$ and $h \equiv \Delta C_p^{max} \propto L^{1.33}$ [7]. Now for a first order transition, we know that finite scaling requires that $h \propto L^d$. So clearly the scaling hypothesis is violated and there is more at work in producing this behavior than finite size effects.

A second type of first order transition is the freezing/melting transition. While this transition has been investigated for many fluids, we will focus on the results for helium, which has not only many of the common features of the transition, but also has the superfluid transition at approximately the same point.

Molz and Beamish [10] found hysteresis in the melting and freezing of ^4He in all three porous media. The behavior was measured via sound velocity and attenuation of the helium in the media. An example of a hysteresis curve (from attenuation data) for each of the media is found in Fig. 2. It is evident that Vycor has the largest hysteresis followed by aerogel and then Anopore which has no appreciable hysteresis. Examining several different pressures resulted in freezing ranges of about $0.2K$ for Vycor, $0.04K$ for aerogel, and $11mK$ for Anopore [10]. This behavior is explained by the increase in pore size from Vycor to Anopore, which is several orders of magnitude, since for a larger pore size the helium is less confined and so closer to the bulk configuration. This idea is agrees with a geometric freezing model

where the liquid-solid interfacial energy leads to freezing point depression inversely proportional to the pore size [10].

From measurements of the freezing and melting hysteresis at several pressures, the phase diagram was determined, as shown in Fig. 3 [10]. As can be seen from the phase diagram, the hysteresis between melting and freezing is quite evident for both porous media. The results from Anopore are not included due to the near lack of hysteresis. Perhaps the most striking feature of the phase diagram is that for some pressures, one passes through the superfluid transition of freezing but not upon subsequent melting. Thus the helium is melting directly into the normal fluid after being frozen in a superfluid state.

Next we will examine several continuous transitions manifested in porous media. First we look at the superfluid transition of ^4He. In the bulk, ^4He undergoes a transition to the superfluid state at a temperature of about $T_c = 2.17K$ at which point the heat capacity diverges. The superfluid fraction ρ_s/ρ rises from zero at T_c to one at $T = 0$. The density and heat capacity have a power law dependence on the reduced temperature t, $\rho_s \propto t^\zeta (t < 0)$ and $C \propto t^{-\alpha}$ where the experimental values of the exponents have been found to be $\zeta = 0.6705 \pm 0.0006$ and $\alpha = -0.01285 \pm 0.00038$ [11].

Now the superfluid transition has be observed in both the materials Vycor and aerogel. In Vycor, it was found that there was a transition at a slightly reduced temperature and that the heat capacity curve became rounded [9]. In Fig. 4 this result is plotted and corresponds to the "Full Pores" meaning that the Vycor was completely saturated with the helium. The superfluid density was found to scale like the bulk system (Fig. 5) with the critical exponent $\zeta = 0.65 \pm 0.03$ [9]. Clearly this result is almost identical to the bulk value, which implies that the two transitions both belong to the same universality class.

The heat capacity has also been measured for ^4He films absorbed in Vycor. These curves are also shown in Fig. 4 and correspond to the various σ values. Examining the graph reveals that for a decreasing amount of helium, the transition temperature

shifts farther toward zero and the peak is increasingly suppressed. The superfluid densities were again found to behave as a power-law with exponents close to the bulk values [9].

In aerogel one also find a superfluid transition in ^4He. The superfluid density and heat capacity for a 94% porosity aerogel is shown in Fig. 6. The superfluid transition occurs as ρ_s vanishes, which occurs at the broad peak in the heat capacity. The spike at the bulk transition temperature arises from a remnant of bulk helium in an open volume or in large voids in the aerogel [9]. The density is found to scale with a power-law (Fig. 7). However, unlike the cases of the bulk and Vycor transitions, the exponent has a much larger value, $\zeta = 0.81$. With corrections for high pressure deviations included, this decreases only slightly to $\zeta = 0.75$ [11]. As this value is still much larger than the bulk exponent, the superfluid transition in aerogel clearly falls outside of the bulk universality class. Furthermore, the heat capacity curve also differs significantly from the bulk case. For temperatures above the critical temperature, the curve appear singular but below the transition, the heat capacity is approximately a linear function of temperature. Hence the exponents for the heat capacity are no longer equal across the transition.

Besides the superfluid transition, ^4He has also been found to have a liquid-vapor critical point in aerogel. Through the use of heat capacity and vapor-pressure isotherm measurements, the coexistence curve was determined [6]. The heat capacity as a function of the temperature is given in Fig. 8. The bulk liquid-vapor transition has a sharp peak in heat capacity as the transition temperature is passed (at the critical density $\rho_c = 0.0696 g/cm^3$). As seen in the figure, in aerogel this peak becomes broadened for densities near the bulk critical density. However, as the ^4He density is increased a sharp peak arises in the broad peak at a temperature below the bulk critical temperature. That this peak corresponds to a non-bulk transition can be seen from curve "IV", as it contains two distinct peaks, one corresponding to the bulk and another to the lower temperature peak [6].

In Fig. 9 the coexistence curve is displayed. Of note is the very small region of

coexistence as compared to the bulk coexistence curve. Now assuming a symmetric coexistence region one may scale it as $frac|\rho_l - \rho_v|\rho_c \propto (-t)^\beta$ where the densities correspond to the liquid, vapor and critical densities respectively and t is the reduced temperature. The curve of Fig. 9 was fit to this scaling form resulting in the values of $T_c = 5.198K$ and $\beta = 0.28 \pm 0.05$ [6]. The bulk values for this form are $T_c = 5.198K$ and $\beta = 0.325$. The β values are found to be in agreement to within the error of the fit. One may interpret this as implying that even in the aerogel the universality class of the system is not changed.

The final experimental system to be investigated is that of binary coexistence of two different species. To begin we examine mixtures of ^3He and ^4He in aerogel. By use of torsional oscillator experiments, the phase diagram of such mixtures in 98% porous aerogel has been determined and is shown in Fig. 10 [11]. In comparing this with the bulk phase diagram (Fig. 11), several differences are evident. The first is that there no longer exists a tricritical point as the coexistence curve for the ^3He-^4He system has detached from the superfluid transition line. The critical ^3He concentration decreased from the bulk value of 0.669 to 0.57 while the critical temperature went from $0.872K$ to $0.85K$ [2]. Perhaps the most striking difference however is a direct result of this shift. In the aerogel, there exists a superfluid state of highly concentrated ^3He that was not possible in the bulk due to the tricritical point.

Similar effects on the coexistence curve as found for ^3He-^4He mixtures can be observed in other binary mixtures. One such example is that of isobutyric acid and water in a silica gel [5]. As seen in Fig. 12, the region of coexistence is much smaller in the concentration of isobutyric acid than in the bulk. As well, the critical temperature is estimated to be below $23\,^\circ C$ which is depressed from the bulk value of $25.722\,^\circ C$.

3 Theoretical Work

A common theme for almost every model of the various phase transitions in porous media involves the use of random fields to describe the effect of the porous media. A typical example is the random field Ising system which has the following Hamiltonian $H = -J\sum_{<ij>} S_i S_j - \sum_i h_i S_i$ where the h_i are the random fields described by some probability distribution [4]. In this section we will examine the calculations and simulations of these types of Hamiltonians and their applications to the experiments above.

To begin we examine some of the theoretical work behind the isotropic-nematic transition of liquid crystals. Two popular models used to describe the systems are the Lebwohl-Lasher (LL) model and the Potts model. Denoting the random field portion of the Ising model above by H_1 the LL model is as follows, $H_0 = H - H_1 = -J\sum_{<ij>} (\mathbf{S_i} \cdot \mathbf{S_j})^2$ where the $\mathbf{S_i}$ are n-dimensional unit vectors. The n-state Potts model has the Hamiltonian $H = -J\sum_{<ij>} \mathbf{s_i} \cdot \mathbf{s_j} - h_0 \sum_i \mathbf{s_i} \cdot \mathbf{h_i}$ where the $\mathbf{s_i}, \mathbf{h_i}$ are vectors which point to the vertices of an n-dimensional tetrahedron [3].

Mean field analysis of these two models with respect to a concentration p of sites with random, infinite field, reveals a first order phase transition at $T > 0$ for all $p \neq 1$ [3]. Monte Carlo simulations of the three-state Potts model resulted in the peak in the specific heat being broadened, shifted to lower temperature, and also reduced in magnitude [3]. This is in agreement with the experimental results given above.

The liquid-vapor transition in porous materials has also been investigated via a grand-canonical Monte Carlo simulations. A "quenched-annealed" system was studied in which two types of particles were present, matrix and fluid particles. The fluid particles interacted as hard spheres with Lennard-Jones tails, while the matrix particles had a purely repulsive interaction [1]. The resulting coexistence curves for several matrix densities can be seen in Fig. 13. For increasing matrix density, the coexistence curve was found to have much narrower range of coexistence. In

addition, the critical density was found to be shifted to lower densities, while the critical temperature was found to decrease for increasing density. These results are in qualitative agreement with the experimental results for ^3He-^4He and isobutyric acid-water mixtures.

These results are also in qualitative agreement with calculations of a bimodally distributed random field Ising mode using Gaussian fields. In the model, the two (up and down states) are separated by a first order line that ends at a critical point [4]. However, the exponent β is found to be close to zero, which does not agree well at all with the experimental value given above (0.28).

4 Conclusions

The subject of phase transitions in porous media has many realizations in experiment. For almost all bulk transitions, a corresponding transition is usually found upon confinement in a porous medium. In many cases the behavior in this medium is even richer that the bulk behavior.

How the behavior of the system changed upon confinement was highly dependent on the type of transition and type of material. For example the superfluid transition in Vycor appears to be in the same universality class as the bulk transition, while the larger porosity medium Anopore does not. However, for freezing melting transitions, Vycor displayed the largest deviation from bulk behavior. Similar effects are found in the other types of systems. Thus it is apparent that to understand the behavior in the porous media, knowledge of the media or bulk transition alone will not be sufficient.

The theories that have been used to explain the above experiments are generally found to be in qualitative agreement. However, quantitative agreement is still quite far from realization in most of the fields. Thus work needs to be done in improving the theoretical models used in analyzing the various systems. As well there are several areas that have not yet been explained, such as the lack of a sharp transition

of superfluid 4^He in aerogel [11]. So more work needs to be done to understand why these anomalies are found.

References

[1] M. Alvarez, D. Levesque, J.-J. Weis, *Phys. Rev. E* **60**, 5495 (1999).

[2] S. B. Kim, J. Ma, M. H. W. Chan, *Phys. Rev. Lett.* **71**, 2268 (1993).

[3] A. Maritan, et. al., *Phys. Rev. Lett.* **72**, 4113 (1994).

[4] M. Cieplak, J. R. Banavar, *Physica A* **194**, 63 (1993).

[5] Z. Zhuang, A. G. Casielles, D. S. Cannell, *Phys. Rev. Lett.* **77**, 2696 (1996).

[6] A. P. Y. Wong, M. H. W. Chan, *Phys. Rev. Lett.* **65**, 2567 (1990).

[7] L. Wu, et. al., *Phys. Rev. E* **51**, 2157 (1995).

[8] J. M. Ryan, P. R. Wamsley, K. L. Bray, *Appl. Phys. Lett.* **63**, 2260 (1993).

[9] J. Reppy, *J. Low Temp. Phys.* **87**, 205 (1992).

[10] E. Molz, J. Beamish, *J. Low Temp. Phys.* **101**, 1055 (1995).

[11] M. Chan, N. Mulders, J. Reppy, *Physics Today* **49(8)**, 30 (1996).

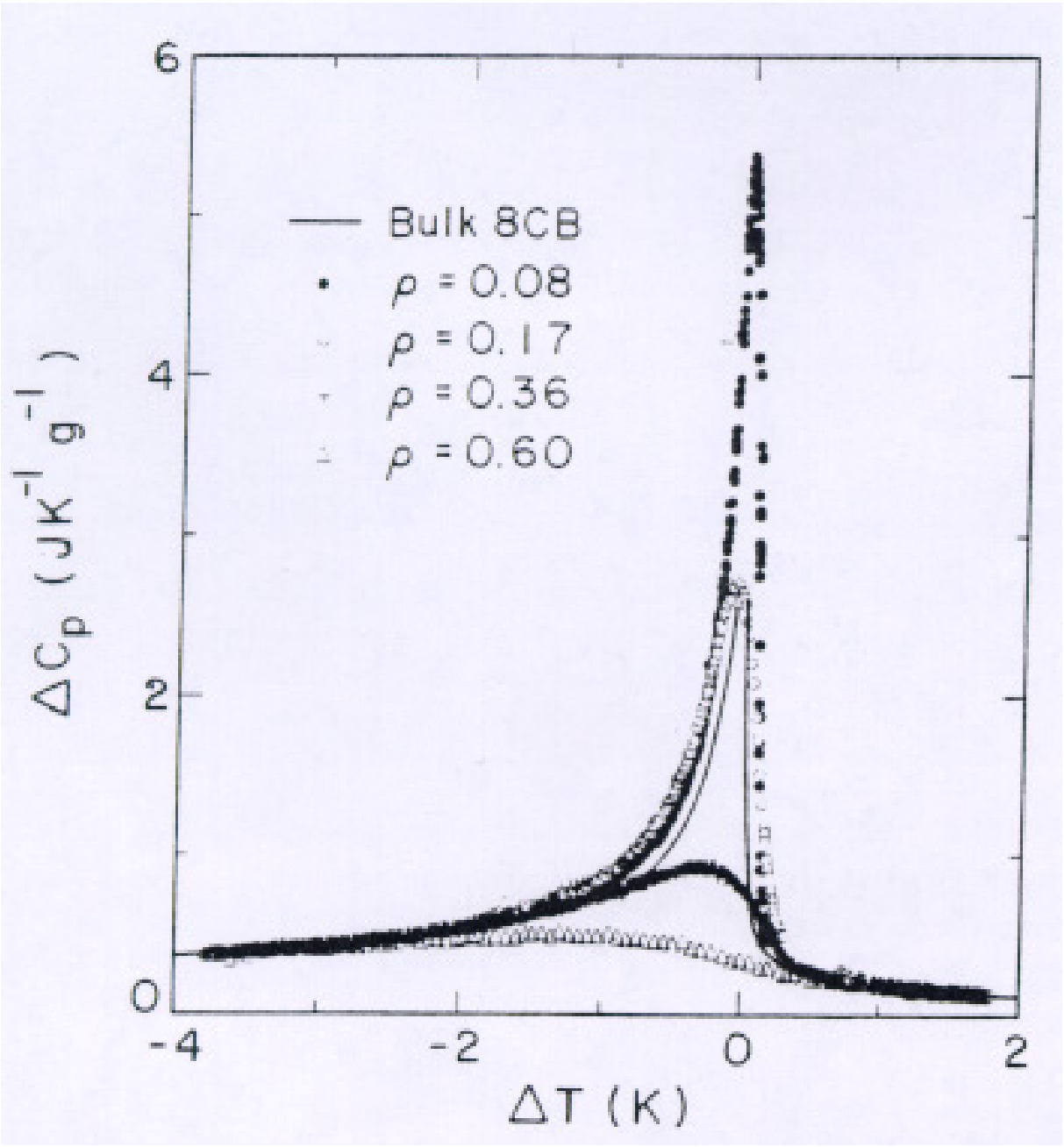

Figure 1:
Excess heat capacity associated with the nematic isotropic transition for bulk 8CB and for 8CB in four aerogels [7].

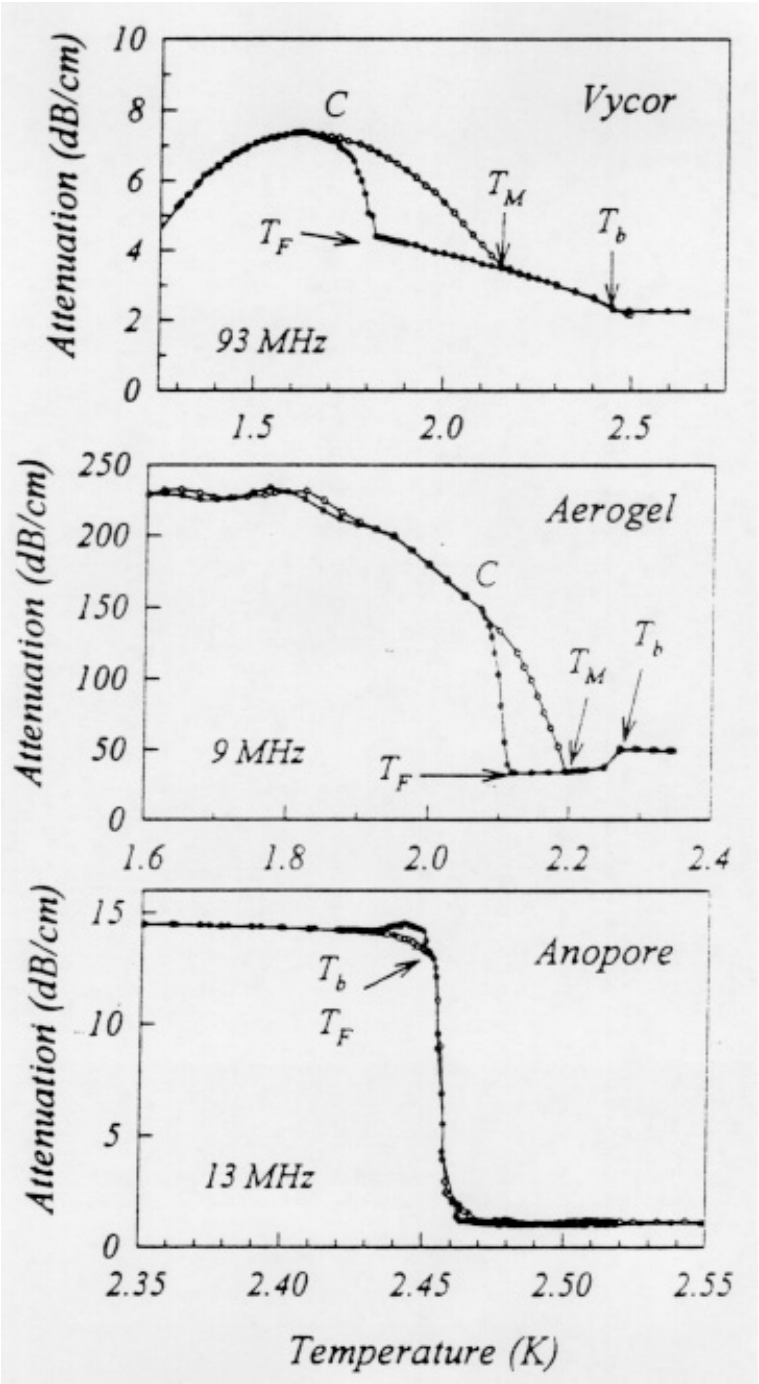

Figure 2:
Freezing/melting hysteresis in sound attenuation. From top to bottom, the data are for Vycor, aerogel, and Anopore samples. T_f marks the onset of freezing during cooling and T_m marks the completion of melting during warming [10].

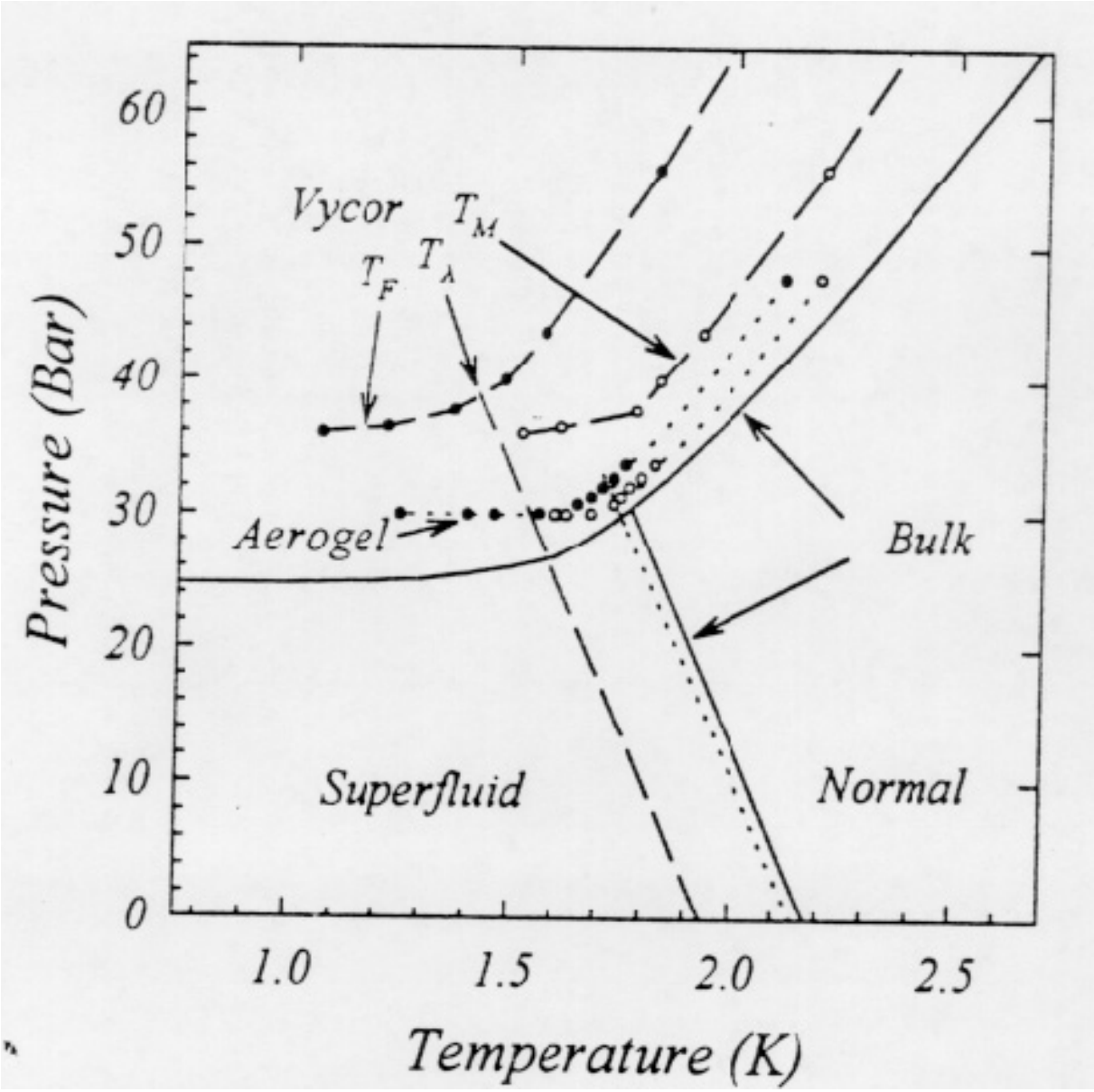

Figure 3:
Phase diagram for ^4He in bulk (solid lines), in Vycor (dashed lines), and in aerogel (dotted lines). The solid symbols mark the onset of freezing, and the open symbols the completion of melting [10].

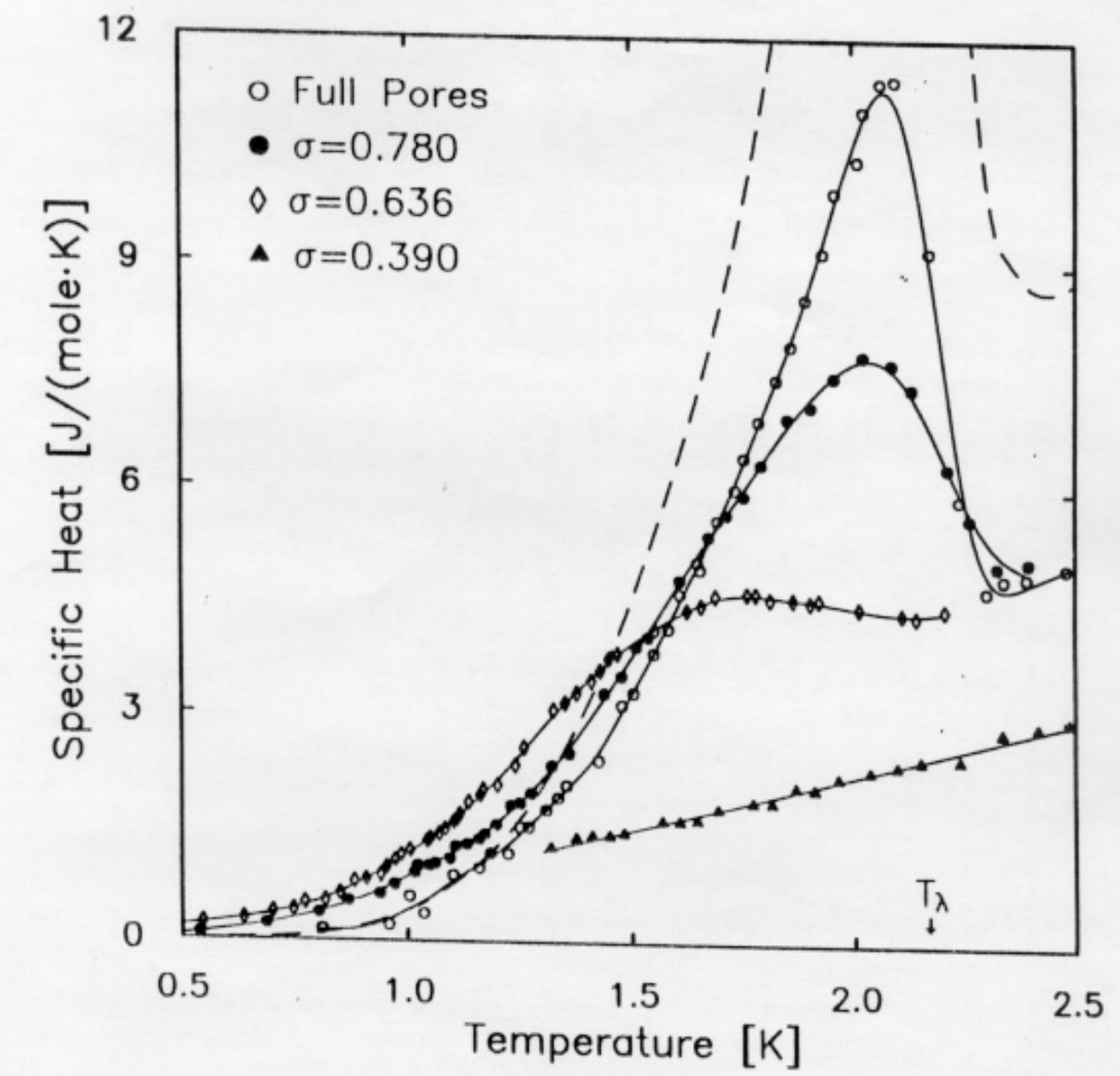

Figure 4:
The specific heat for ^4He in Vycor is shown as a function of temperature for the full-pore case and for three different film coverages. The fractional filling of the Vycor sample is indicated for each film coverage. The specific heat for bulk helium at saturated vapor pressure is indicated by the dashed line [9].

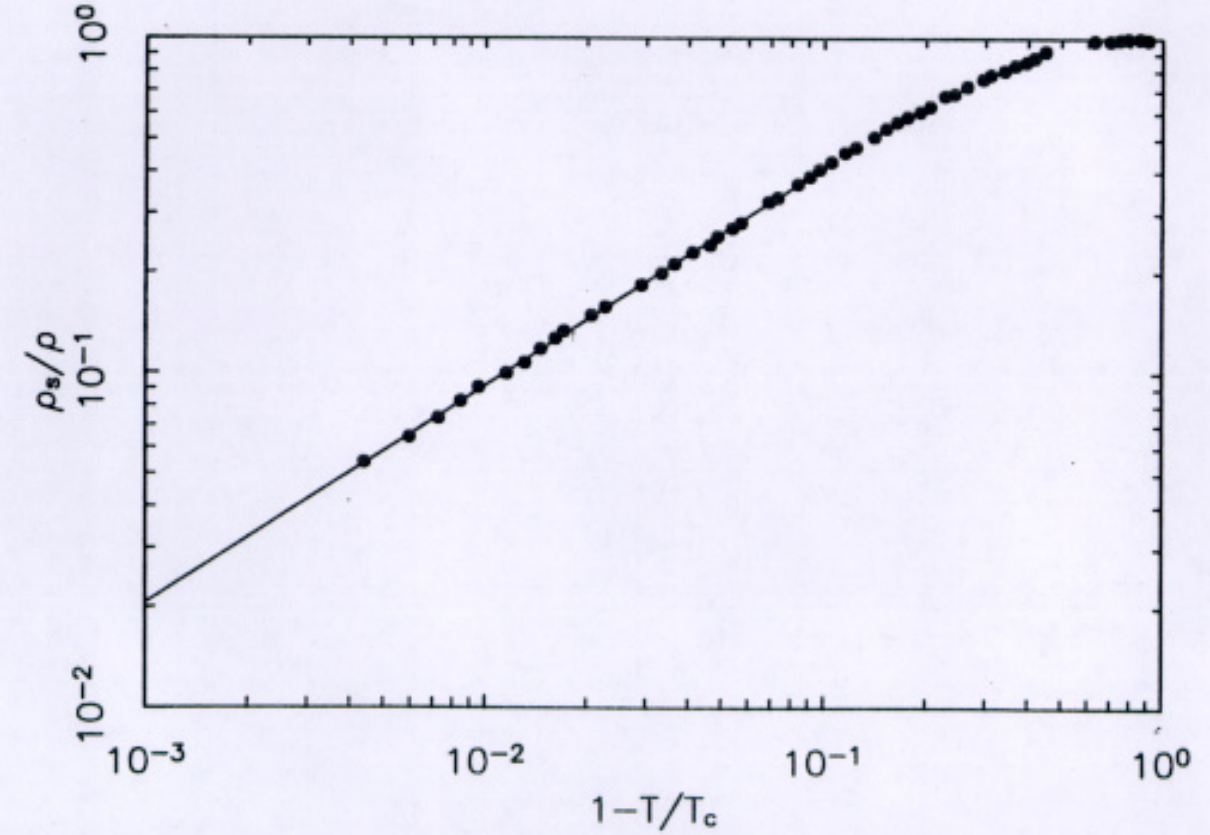

Figure 5:
The superfluid density ratio is shown on a log-log scale as a function of reduced temperature for $T_c = 1.955K$ [9].

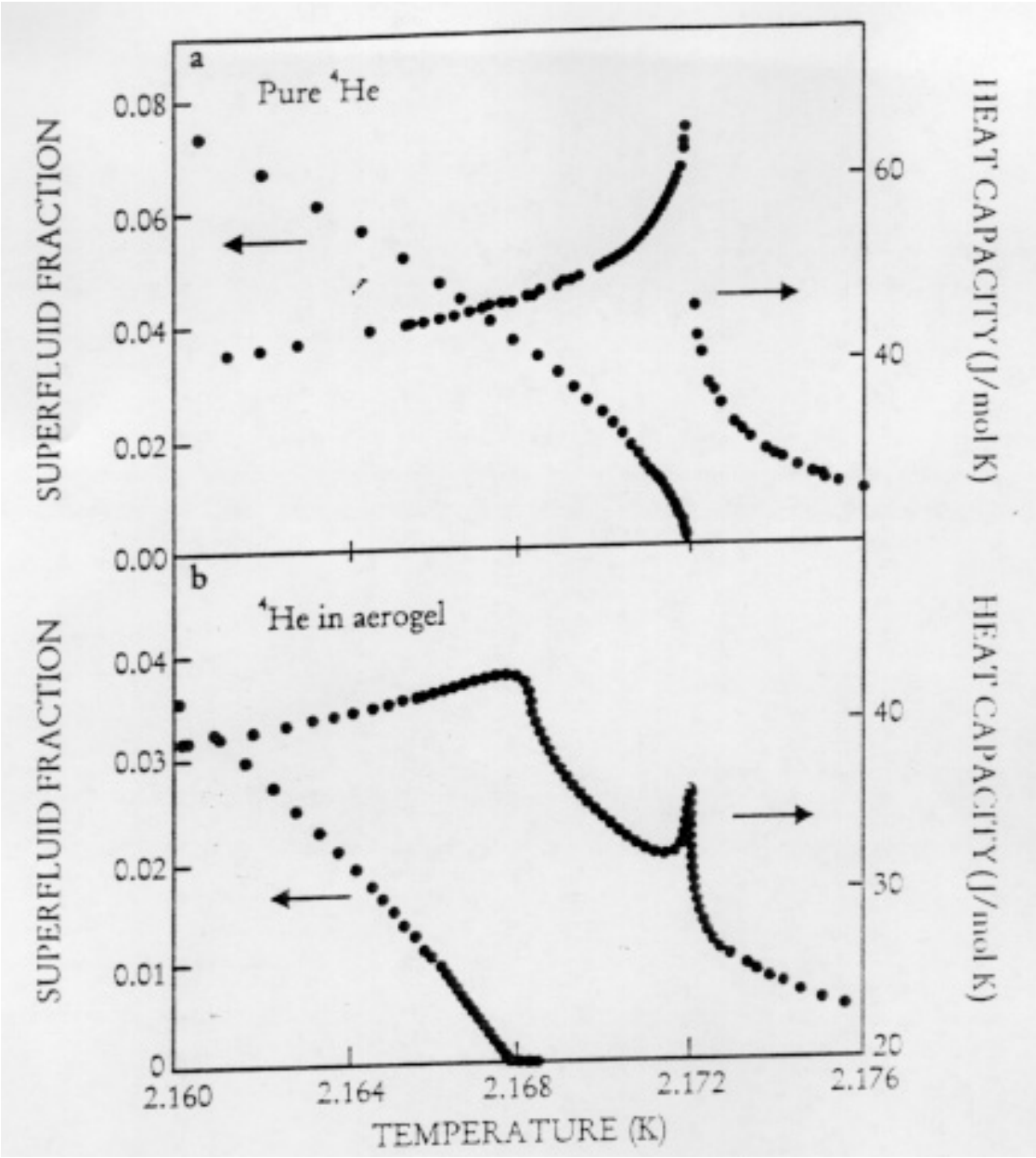

Figure 6:
Plotted are the superfluid fraction and heat capacity of ^4He near the superfliud transition of pure ^4He (a) and of ^4He in aerogel of 94% porosity (b) [11].

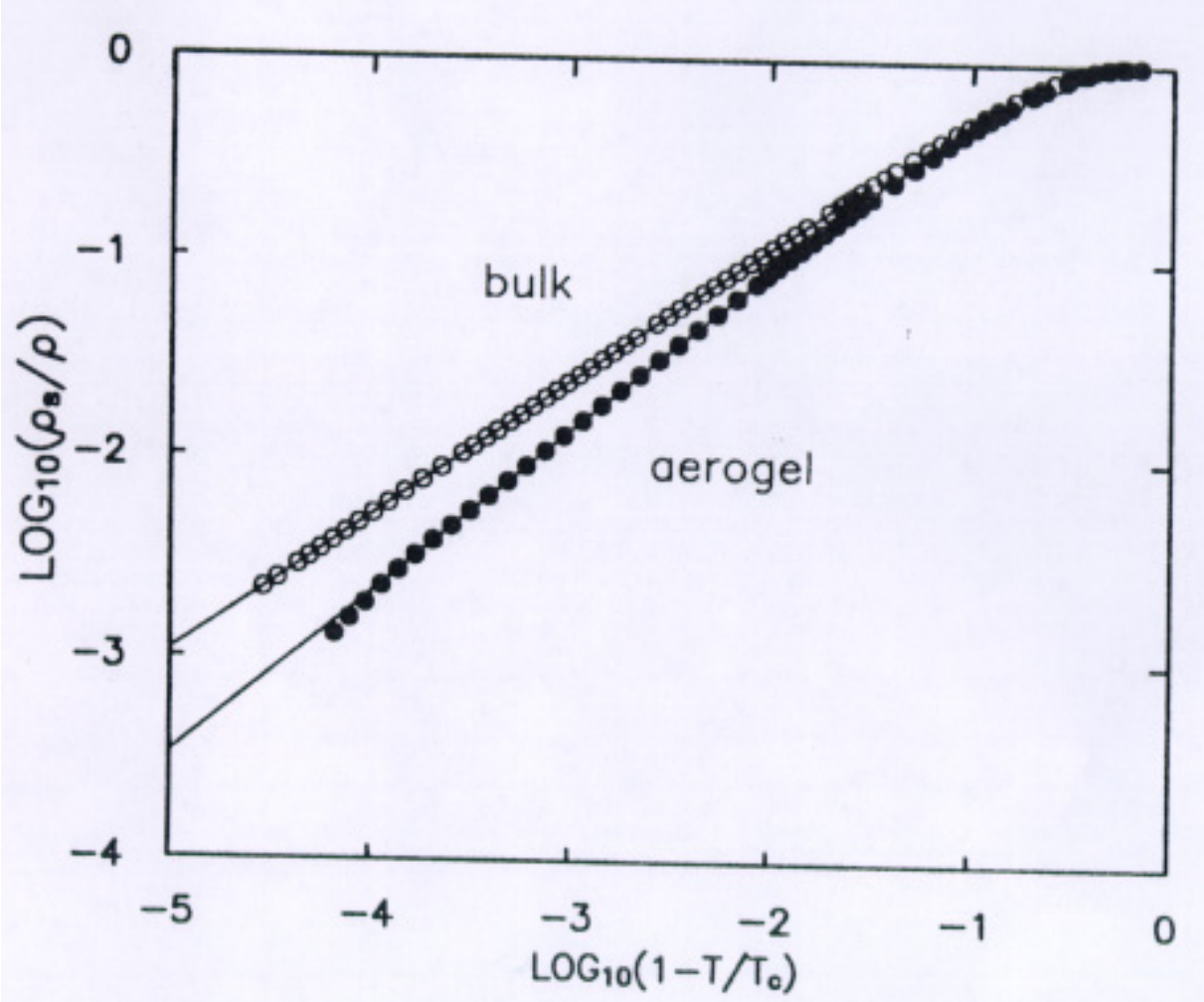

Figure 7:
The power law dependence of the superfluid density near T_c for the bulk helium and aerogel samples is shown [9].

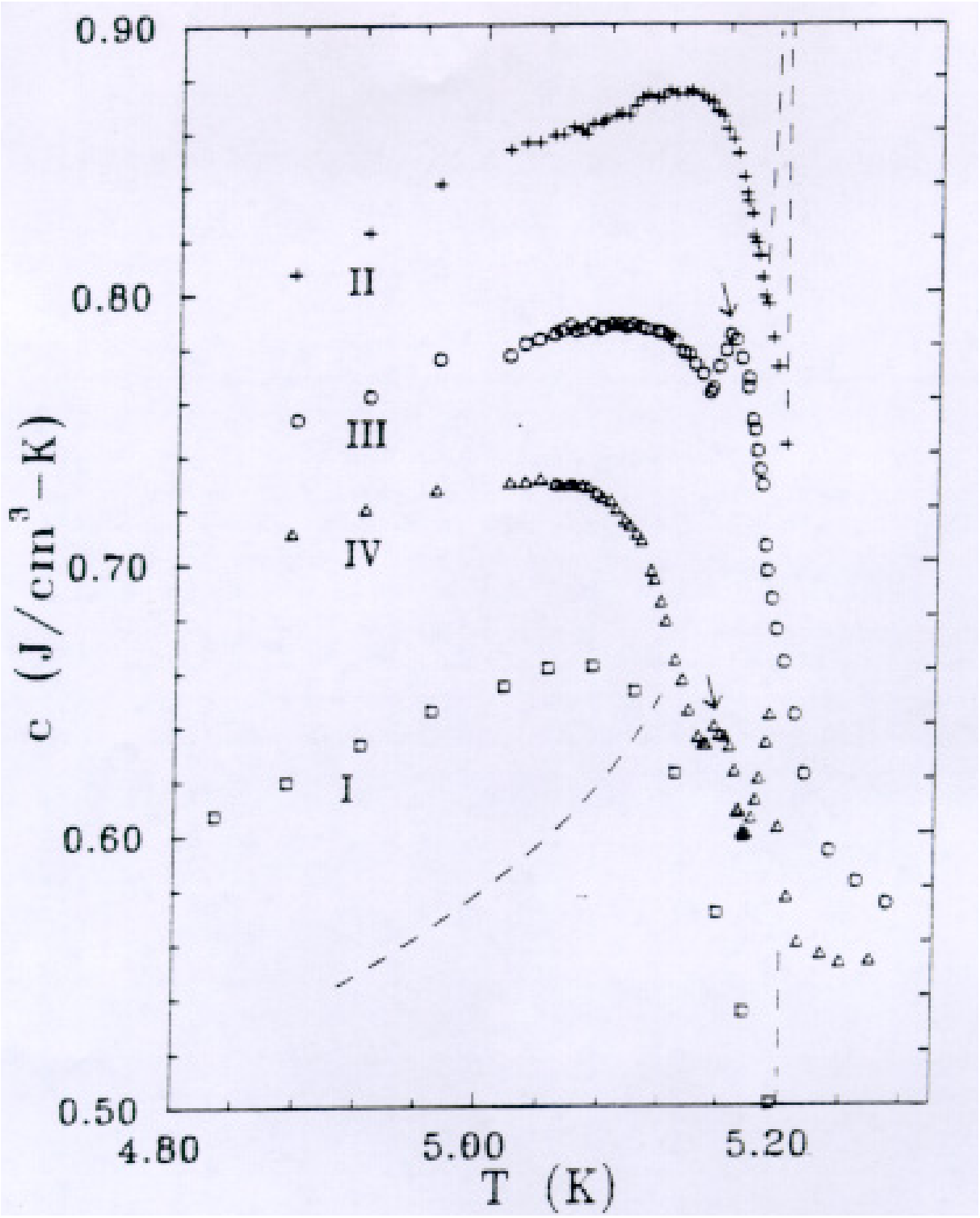

Figure 8:
Specific heat as a function of temperature at four different average densities of ^4He. Arrows indicate the sharp peaks found for ^4He in aerogel. The dashed lines show the specific heat for bulk ^4He near $\rho_c = 0.0696 g/cm^3$. The curves I, II, and IV have been shifted up and down respectively for clarity the ρ for the four curves are 0.0682, 0.0768, 0.0802, and 0.0818 for I,II,III,and IV respectively [6].

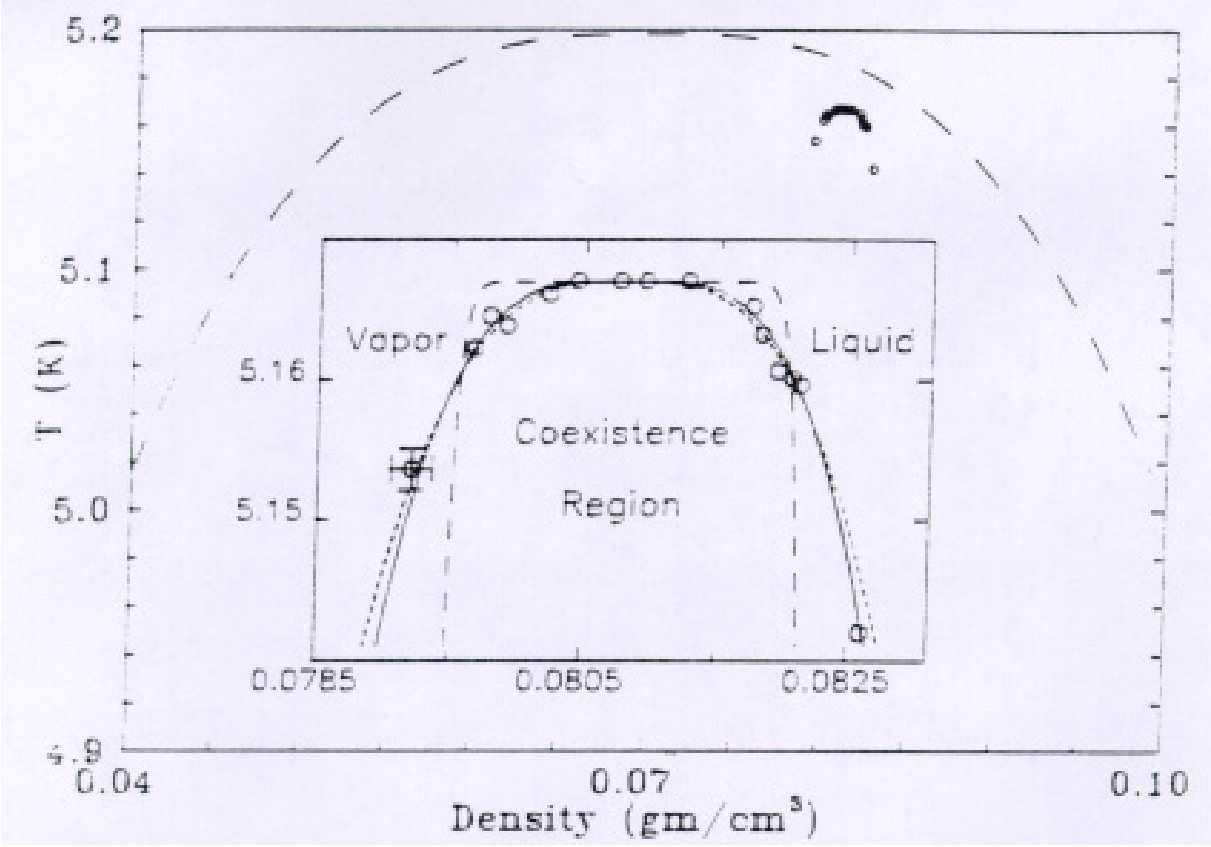

Figure 9:
Coexistence curve of liquid-vapor critical point of ^4He in aerogel. The circles depict the locations of sharp heat-capacity peaks related to the crossing of the coexistence boundary. Both the liquid and vapor densities found here include enhancement effects in aerogel. The dashed line is that of bulk ^4He. The inset magnifies the coexistence boundary in aerogel. The Solid and dotted line show fits to this data [6].

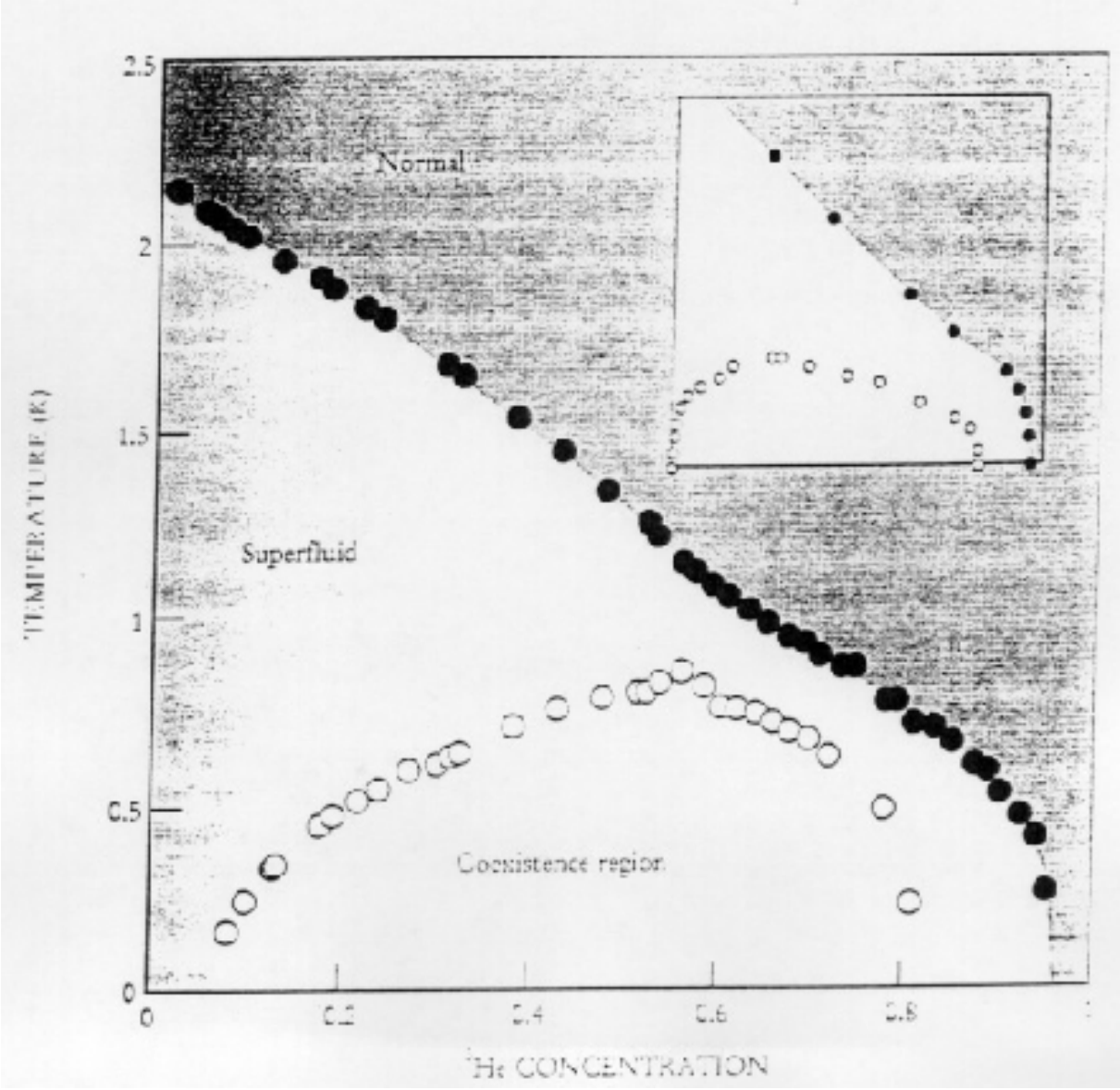

Figure 10:
Measured and Calculated (inset) phase diagrams of ^3He-^4He mixtures in aerogel of 98% porosity [11].

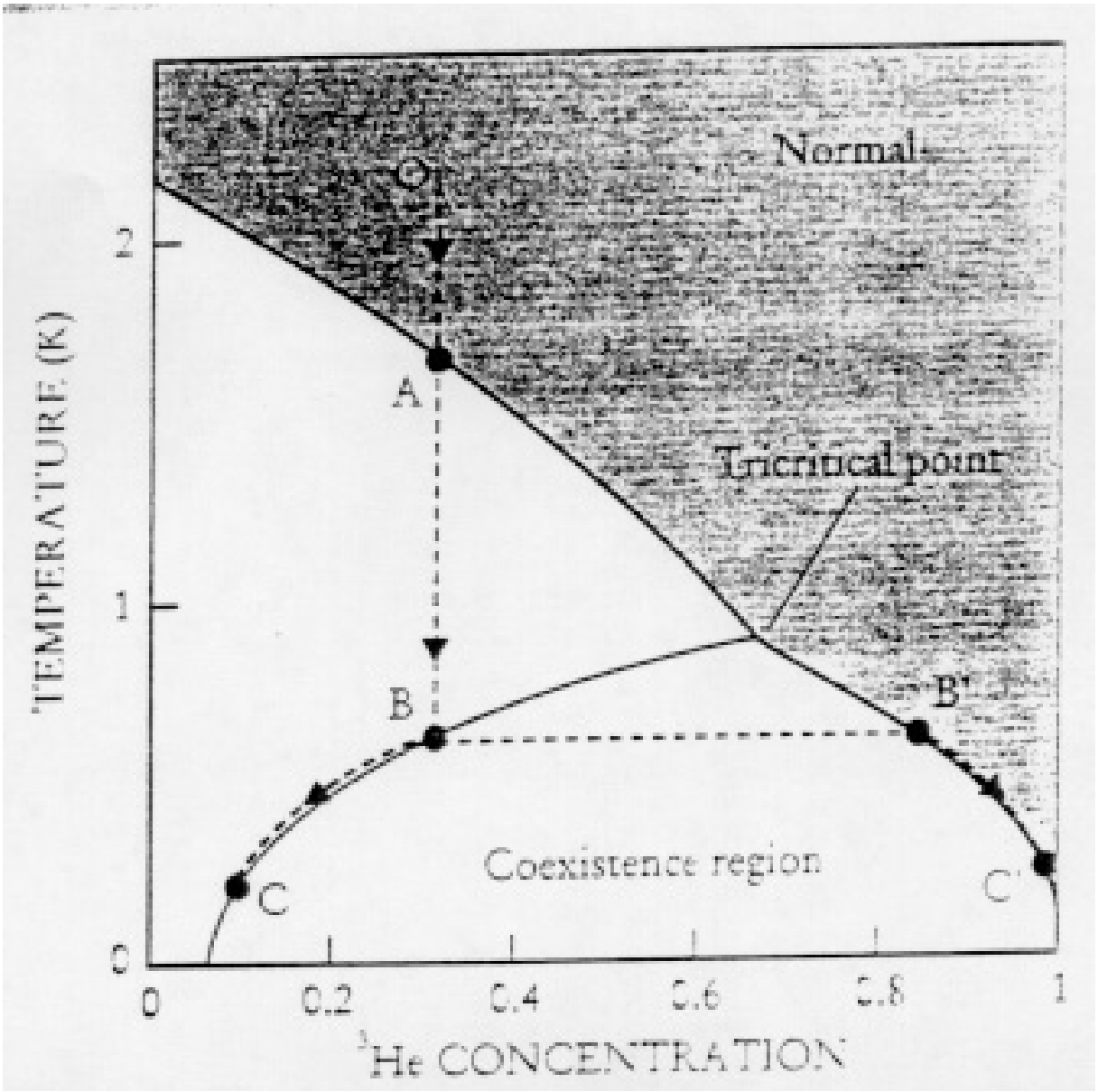

Figure 11: Phase diagram of ^3He-^4He mixture in the bulk [11].

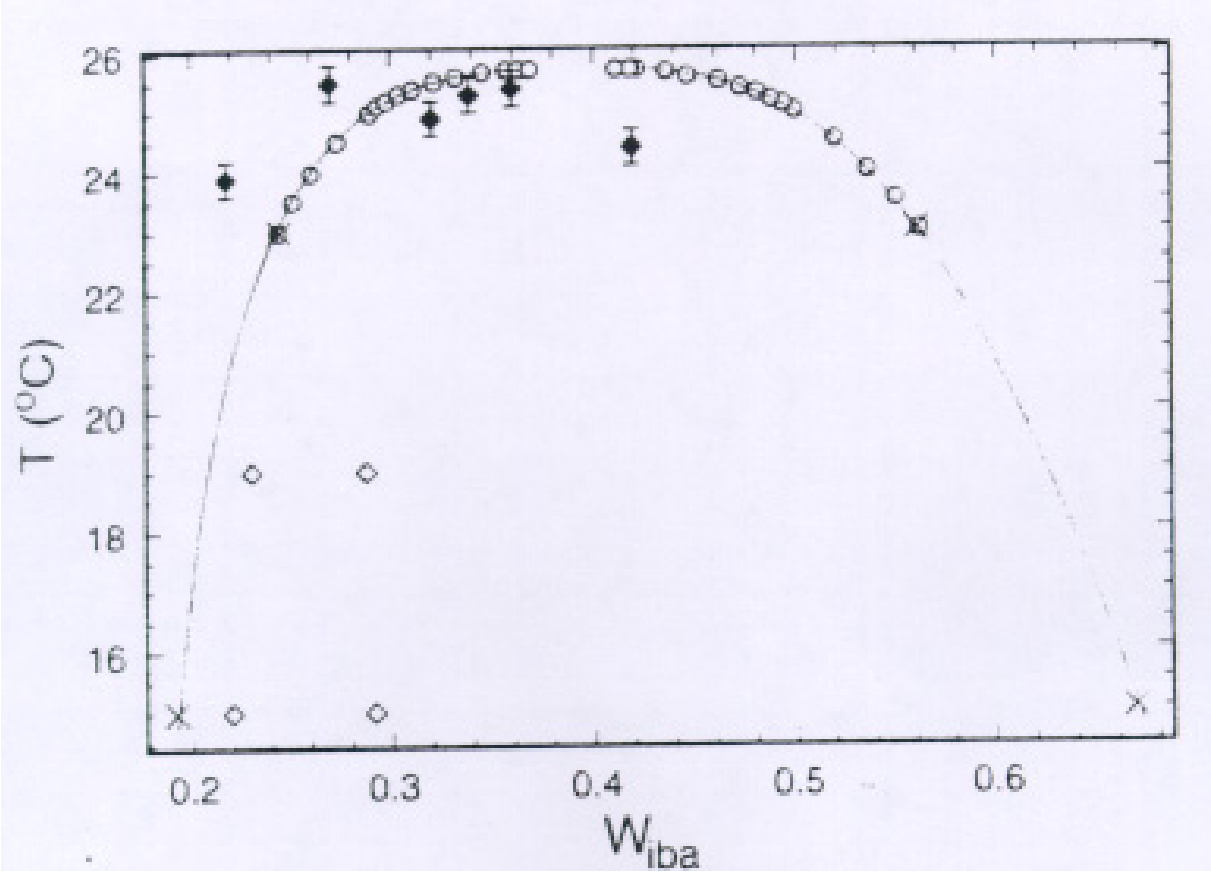

Figure 12:
Phase diagram showing the relationship between the coexistence curve of the pure mixture (open circles, crosses), the narrow two-phase region of the gel/mixture system, which lies between the open diamonds, and the slow mode onset temperature (solid diamonds) [5].

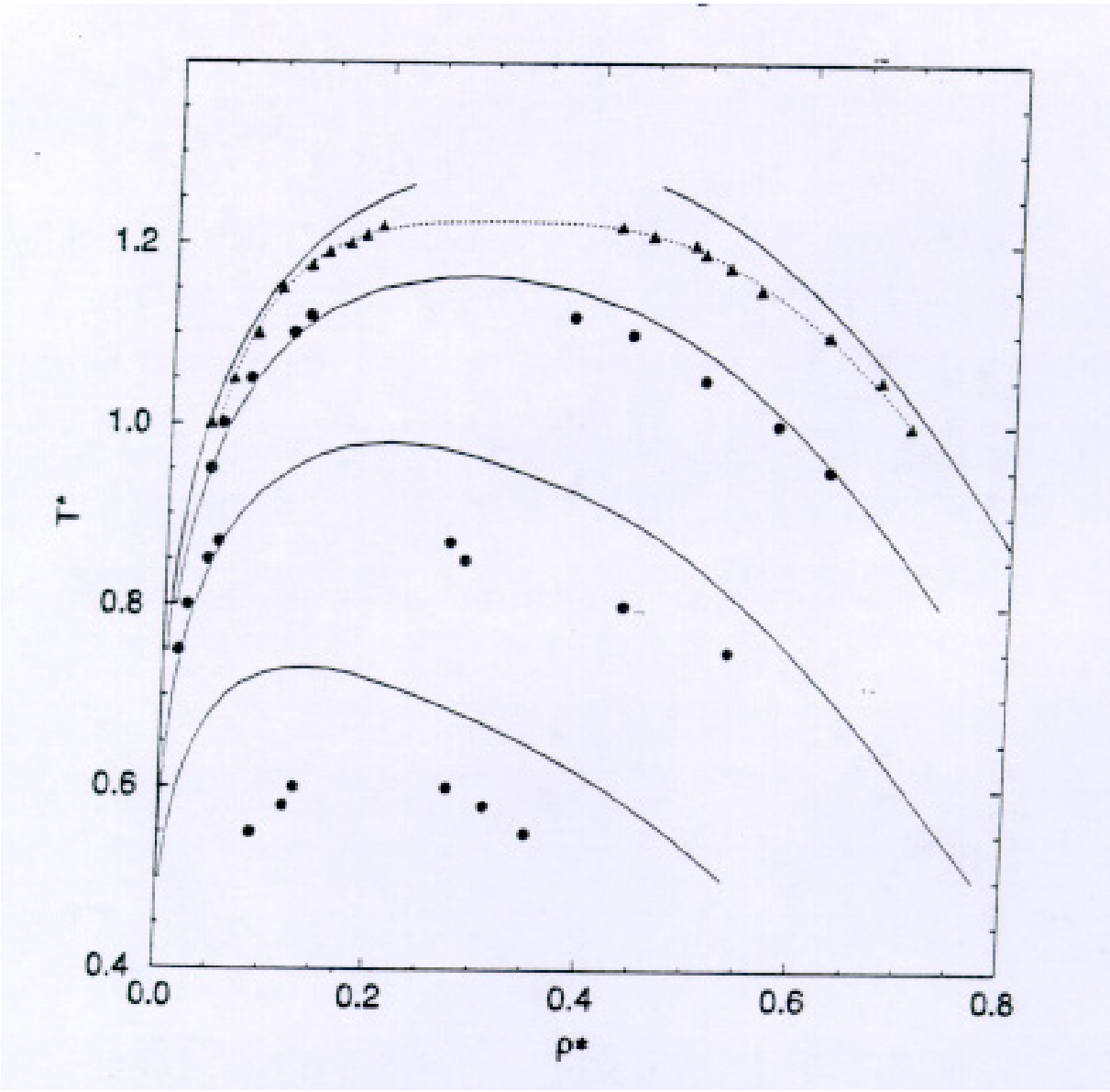

Figure 13: Coexistence curves for matrix densities 0 (bulk),0.046, 0.15, and 0.30 (from top to bottom). Results at finite matrix density are for volume $V = 500\sigma^3$ [1].